Reinterpretation of the GaAsP far-infrared spectra within the framework of the Verleur and Barker model of the alloy phonon spectra

ARTICLE *in* PHYSICA STATUS SOLIDI (B) · AUGUST 2013

Impact Factor: 1.49 · DOI: 10.1002/pssb.201248365

3 AUTHORS, INCLUDING:

Mariusz Woźny
Rzeszów University
5 PUBLICATIONS **6** CITATIONS
SEE PROFILE

E. M. Sheregii
Rzeszów University
142 PUBLICATIONS **357** CITATIONS
SEE PROFILE

Reinterpretation of the GaAsP far-infrared spectra within the framework of the Verleur and Barker model of the alloy phonon spectra

J. Cebulski[*1,2], M. Woźny [1], and E. M. Sheregii[1]

[1] Institute of Physics, University of Rzeszów, Rejtana 16a, 35-310 Rzeszów, Poland.
[2] H. Niewodniczański Institute of Nuclear Physics, Polish Academy of Sciences, Radzikowskiego 152, 31-342 Kraków, Poland as visiting scientists..

Received XXXX, revised XXXX, accepted XXXX
Published online XXXX

Key words: Phonon spectra, Kramers-Kronig transformation, alloys compounds

[*] Corresponding author: e-mail cebulski@univ.rzeszow.pl, Phone: +48-17-8721153, Fax: +48-17-8721263

In this research the model of five basic structural units (tetrahedra) proposed by H. W. Verleur and A. S. Barker [H. W. Verleur and A. S. Barker, Phys.Rev. **149**, 715 (1966)] (VB-model) is completed by the statistical approach, which enables us to derive quantitative relations for the oscillator strengths of separate lines. The rule of proportionality of the oscillator strength sum to the content of the components for each dipole pair is developed as a criterion of random distribution of atoms in the lattice. Thus, a proper identification of observed lines was performed. It is shown that the optical-reflection spectra obtained experimentally by the VB-model authors for GaAsP solid solutions can be successfully explained using the VB-model, without the hypothesis of clustering of binary GaAs - as well as GaP - tetrahedra, which they introduced.

1 Introduction The paper of Verleur and Barker (VB)[1] is one of the basic and thus most important publications in the domain of phonon spectra of mixed crystals. The subtle structures of the two main GaAs-like as well as GaP-like sub-bands observed for GaAsP alloys were explained using the model of five basic structural units (tetrahedra) T_n where n is number of the As-atoms in the tetrahedron (the number of other anion P-atoms in the tetrahedron is 4-n, respectively). Since then, this model has been widely used for interpretation of the semiconductor alloy phonon spectra[2–18] as well as the EXAFS data[19–22]. Thus, the work of VB[1] is important, because the authors not only proposed the model of the five basic structural units for the explanation of the solid solution phonon spectra, but simultaneously introduced a correction of this model: a so-called clusterization factor β. This factor removes the random distribution of the tetrahedra in the lattice of the solid solution and later inspired the site occupation preference theory (SOP-theory)[19–21]. Recently, the reflection spectra obtained by VB[1] were reinterpreted using an "ab initio" calculation[23] and a criticism of the "clusterization model" in the form introduced by VB, was also presented. Therefore, to give some order to the terminological chaos, it is necessary to underline, that the main aim of the VB work[1] was the presentation of the five basic structural units (tetrahedra T_n) model. Moreover, the clusterization factor, which was introduced by the authors, is not necessary for the interpretation of the reflection spectra features in the new approach to the VB model, as will be shown in this paper.

This new approach, described in the present paper, previews using the imaginary part of the dielectric function obtained by the Kramers-Kronig (K-K) transformation applied to the reflection spectra of the GaAsP alloys mea-

sured by VB. VB interpreted the reflection spectra directly by calculating the reflection coefficient R(ω) according to the following formula:

$$R(\omega) = \left|(\sqrt{\epsilon(\omega)} - 1)/(\sqrt{\epsilon(\omega)} + 1)\right|^2 \qquad (1)$$

where $\epsilon(\omega)$ is the dielectric function calculated by VB using the classical oscillator method based on their five tetrahedra model. This interpretation method enables us to distinguish different aspects of the analysis supported by the measured data. On one hand, one encounters an essential problem concerning weak resonances, which could be hidden as weak shoulders in the R(ω) curves. On the other hand, the curve of the imaginary part of the dielectric function Im$\epsilon(\omega)$, obtained by the Kramers-Kronig transformation from experimental reflection spectra R(ω), reveals weak features on the spectra and can be interpreted clearly by applying Lorentzians. This enables us to determine precisely the phonon mode frequencies: in the case of the imaginary part of the dielectric function they correspond to the positions of the maxima, for the real part of the dielectric function they are represented by the position of the zero. A similar method is numerical differentiating of the reflectance data as is shown in Appendix B, while the Kramers-Kronig transformation is an integration of the same data. This is important in the case of spectral data obtained in the 60's of previous century, before the time of the modulation spectroscopy [24]. Therefore, both - the imaginary and real parts of the dielectric function, Im$\epsilon(\omega)$ and Re$\epsilon(\omega)$ - must be analyzed simultaneously.

The second advantage of this approach, is the fact, that the amplitudes of resonances in the Im$\epsilon(\omega)$ curves are proportional to the oscillator strengths. In the case of solid solutions phonon spectra, the last oscillator strengths can be described statistically, which justifies quantitative identification of the observed lines, as will be shown in this paper.

In the present paper, we report the calculation method of the real and imaginary part of the dielectric function from the reflectance curves published by VB[1]. Furthermore, the obtained Im$\epsilon(\omega)$ curves are interpreted and compared with the interpretation based on Re$\epsilon(\omega)$ presented in the Appendix. Based on these evaluations, a description of the VB model for the random distribution of atoms in an alloy lattice is presented. In addition, the main relationship for the probability of finding atoms in the lattice as well as for the oscillator strengths sums is derived. Finally, we identify the observed lines.

Table 1 Values of dielectric constants for the GaAs and GaP binary compounds averaged on the literature data.

	ϵ_0	ϵ_∞	$\epsilon_0 - \epsilon_\infty$	References
GaAs	12.67	10.6	2.07	26-32
GaP	11.11	9.11	2.0	33-36

2 Calculation of the $Im\epsilon(\omega)$ curves and approximation by Lorentzians The published R(ω) - curves for the five compositions ($y = 0.01$; 0.15; 0.44; 0.72 and 0.94) of the $GaAs_yP_{1-y}$ alloys[1] were scanned and digitalized using the LabView programming environment. GaAsP is known to have a negligible concentration of free carriers. Therefore, in an attempt to treat the measured reflection spectra R(ω, y) of semi-insulator materials in a reproducible way, as well as minimizing uncertainties due to subjective manual intervention, we strictly followed the subsequently described rough procedure. For insulator materials the soft wing of each spectrum is extended until $\omega = 0$ using the function f$(\omega) = A(0) + B(0)exp(\xi(0)\omega)$ to coalesce on one hand the end of the R(ω) curve as $R(0) = \left|(\sqrt{\epsilon_0} - 1)/(\sqrt{\epsilon_0} + 1)\right|^2$, and the soft wing of the available phonon spectrum, on the other. In the high-frequency region, in order to coalesce the soft wing of the electron structure resonances with the far-infrared reflectance curve, a similar function f$(\omega) = A(\infty) + B(\infty)exp(\xi(\infty)\omega)$ (see also Ref. [25], pp. 42-46) was applied. The best-fit procedure is used also in this case, for the value of $R(\infty) = \left|(\sqrt{\epsilon_\infty} - 1)/(\sqrt{\epsilon_\infty} + 1)\right|^2$ to the soft wing of the reflectance band in the high-frequency region caused by the inter-band electron transitions. Hence, the extended curve R(ω, y) was included in the K-K integral. In Appendix A the above described procedure is presented, together with the results of K-K calculation i.e. the Re$\epsilon(\omega, y)$ and Im$\epsilon(\omega, y)$ curves in the far-infrared region for the composition with y = 0.01. It is shown, that the above described procedure of the K-K calculation is satisfactory, even if the whole reflectance curve caused by the electron band-structure resonances in the high-frequency region (above 30 000 cm^{-1}) is not included in the K-K transformation procedure (only the left wing of the first resonance).

The two extreme values $\epsilon_0(y)$ and $\epsilon_\infty(y)$ are taken as linear average functions of the composition y of the corresponding component binary values ${}^{GaAs}\epsilon_0$, ${}^{GaAs}\epsilon_\infty$, ${}^{GaP}\epsilon_0$, ${}^{GaP}\epsilon_\infty$ taken from the literature (see Tab. 1), namely, $\epsilon_0(y) = (1-y)^{GaP}\epsilon_0 + y^{GaAs}\epsilon_0$ and $\epsilon_\infty(y) = (1-y)^{GaP}\epsilon_\infty + y^{GaAs}\epsilon_\infty$. This approximation introduces an uncertainty estimated to be, at worst, $< 3\%$ over the composition y-range. Thus, each extended reflection-spectrum was treated by the K-K transformation calculated by a program supplied by Bruker[37]. The real Re$\epsilon(\omega, y)$ and the imaginary Im$\epsilon(\omega, y)$ parts of the dielectric function were obtained in absolute units with a reproducibility within the range of 3% uncertainty[38].

The curves of Re$\epsilon(\omega, y)$ and Im$\epsilon(\omega, y)$ parts obtained by this method for five compositions of the GaAsP-alloys described above, are collected in Fig. 1 (a),(b). It can be seen, that the Re$\epsilon(\omega)$ curves correspond very well to the maxima observed on the Im$\epsilon(\omega)$ curves: the crossings of zero on the real part corresponds precisely to the positions of maxima on the Im$\epsilon(\omega)$ curves. A spectral analysis was applied to these curves using a sum of Lorentzians:

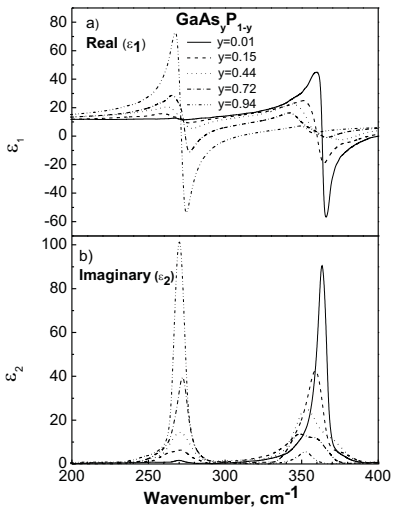

Figure 1 The Re $\epsilon(\omega, y)$ and Im $\epsilon(\omega, y)$ parts of the curves obtained for $GaAs_yP_{1-y}$ by K-K transformation from the reflection R(ω) - curves measured by V-B and published in Ref. 1: (a) Re $\epsilon(\omega, y)$ curves; (b) Im $\epsilon(\omega, y)$ curves.

$$Im\epsilon(\omega) = \sum_{i=1}^{k} \frac{S_i \gamma_i \omega}{(\omega_{TOi}^2 - \omega^2)^2 + \omega^2 \gamma_i^2} \qquad (2)$$

where S_i, ω_{TOi} and γ_i are the oscillator strength, frequency and damping parameter of the i-phonon mode, respectively. We applied Lorentzians to interpret the observed lines only on the Im$\epsilon(\omega, y)$ or Re$\epsilon(\omega, y)$ curves. Therefore, the positions of these lines determined ω_{TOi}, while the amplitudes of the lines determined S_i. The damping parameter γ_i in the Lorentzians could be assumed as a fitted parameter, but only with limited certainty, because this parameter influences not only the broadening of the lines, but also their amplitude. The Im$\epsilon(\omega, y)$ functions are presented in Fig. 2 (a), (b), (c), (d) and (e) (solid bold curves) with Lorentzians (thin solid curves) approximating the observed individual lines. The calculated sums of Lorentzians are shown for each composition as bold dotted curves - the best fitting of the Im$\epsilon(\omega, y)$ curves. The Re$\epsilon(\omega, y)$ curves approximated by Lorentzians are presented in Appendix B in Fig 6 (a), (b), (c), (d), and (e). The mean-square deviations between theoretical curves and experimental ones (the curves of the Im $\epsilon(\omega, y)$ as well as the Re$\epsilon(\omega, y)$ curves obtained from experimental reflectance data) are presented for each composition in Fig. 2 and 6. The approximation was performed using a specially written program in the LabView programming environment and the mean square deviation was calculated automatically for each curve. The approximation of the Im$\epsilon(\omega)$-curves is not best fitting with 3xN parameters, where N is the number of Lorentzians applied for approximation. Therefore, we do not have the possibility to choose freely the parameters of Lorentzians for approximating the Im$\epsilon(\omega)$ - curves. Paradigm " We applied Lorentzians to interpret the observed lines only..." forces us to find real values at the oscillator parameters corresponding to the experimentally observed lines.

The positions of each interpreted line-oscillator on the frequency scale ω_{TOi} are shown in Fig. 3 as filled circles for GaAs-like modes in the region 240 - 280 cm^{-1} and as filled squares for GaP-like modes in the region from 330 to 365 cm^{-1}. The sizes of circles and squares reflect the oscillator strengths of each mode. Beside these modes two additional ones, marked by open circles and squares, are observed outside the two discussed regions. These lines are clearly observed on the Im$\epsilon(\omega, y)$ curves for y = 0.15 and for y = 0.44 and cannot be ignored. It is shown in Figures 2 and 3, that for samples with a composition varying between $0.15 \leq y \leq 0.72$ the number of lines observed is superior or is equal to 8 (y = 0.72) while for y = 0.01 and y = 0.94 this number is equal to 5.

3 Interpretation within the framework of the V-B model

3.1 Description of the V-B model in the case of random distribution To interpret the lines observed on the basis of the VB model it is necessary to remember, that a zinc blende crystalline structure is characterized by basic tetrahedra, each with a central ion surrounded in the first coordination shell by four nearest neighbors (NN) at the vertices. In the AY_yZ_{1-y} ternary zinc blende structures several tetrahedron configurations T_n (n is the number of Y-atoms in the tetrahedron) coexist simultaneously: 2 strictly-binary corresponding to the AZ and the AY compounds whose lattices are characterized by the tetrahedron units T_0 and T_4 (configurations) respectively, and 3 strictly-ternary, i.e., characterized by the configurations T_1, T_2 and T_3.

In an ideal crystal lattice all these tetrahedral configurations generate at least (2 x 1) + (3 x 2) = 2 + 6 = 8 optically-active phonon modes. Thus, eight different lines could be observed in the experimental phonon spectra, as a subtle structure of two bands, AZ-like and AY-like. These are the canonical phonon modes (CPMs) some of which, as mentioned above, appeared as a fine structure of two bands. The probability to find the T_n configuration in an ideal lattice of the AY_yZ_{1-y} ternary solid solution, can be found using the Bernoulli polynomial (assuming a random atom distribution)[39]:

$$P_y(n) = \binom{4}{n} (1-y)^{4-n} y^n \qquad (3)$$

where $\binom{4}{n} = \frac{4!}{n!(4-n)!}$ is the number of combinations with n elements in the four sets. The probabilities of finding in the lattice anions Y or Z belonging to each tetrahedra T_n, are:

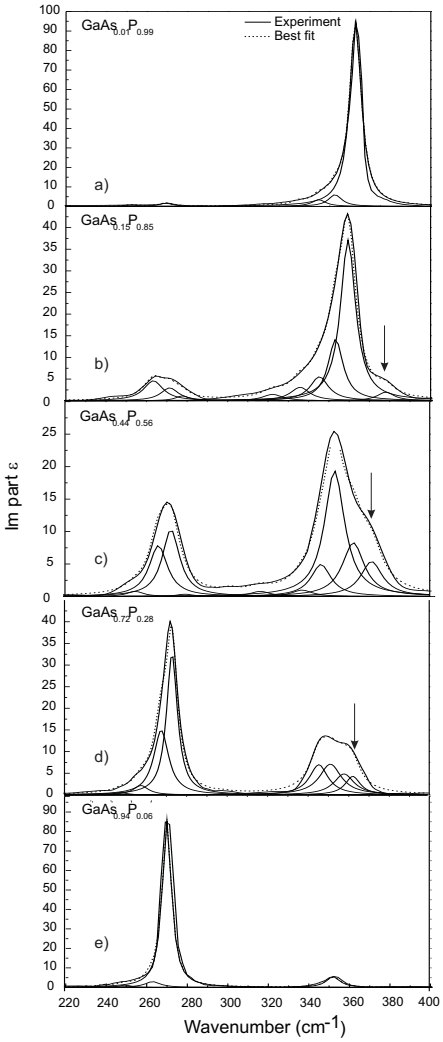

Figure 2 Imaginary parts of the dielectric function Im$\epsilon(\omega, y)$ (solid bold curves): (a) y=0.01; (b) y=0.15; (c) y=0.44; (d) y=0.72; (e) y=0.94. Thin solid curves are Lorentzians applied for the approximation of the Im$\epsilon(\omega, y)$ curves, bold dotted curves - sum of Lorentzians according Eqn. (2). The parameters of Lorentzians are presented in Table 2. P(x^2) is the summarized square deviation for performed approximation. The mean square deviation of the experimental curves[1] after KK transformation and the curve fitting are: (a) $\sigma = 3.21$, (b) $\sigma = 1.11$, (c) $\sigma = 0.67$, (d) $\sigma = 0.94$, (e) $\sigma = 5.21$.

$$P_y^Y(n) = \frac{n}{4}\binom{4}{n}(1-y)^{4-n}\,y^n \tag{4}$$

$$P_y^Z(n) = \frac{4-n}{4}\binom{4}{n}(1-y)^{4-n}\,y^n \tag{5}$$

It is easy to determine that

$$\sum_n^4 P_y^Y(n) = y \tag{6}$$

$$\sum_n^4 P_y^Z(n) = 1-y \tag{7}$$

The oscillator strength of the vibrational mode generated by an A-Z- or an A-Y-dipole in the T_n configuration is[7,20]:

$$S_y^{A-Y}(n) = f_{AZ}N_0P_y^Y(n); S_y^{A-Z}(n) = f_{AZ}N_0P_y^Z(n) \tag{8}$$

where f_{AZ} is the oscillator strength of the single dipole A-Z-pair, N_0 is the number of all dipole pairs (A-Y and A-Z) in the solid solution crystal. The probabilities $P_y^Y(n)$ and $P_y^Z(n)$ where already determined by equations (4) and (5) respectively. At the same time the oscillator sum rule[40] can be derived:

$$\sum_n S_y^{A-Y}(n) = \sum f_{AY}N_0P_y^Y(n) = f_{AY}N_0\sum P_y^Y(n) = f_{AY}N_0y \tag{9}$$

Analogically for A-Z-dipoles:

$$\sum_n S_y^{A-Z}(n) = \sum f_{AZ}N_0P_y^Z(n) = f_{AZ}N_0\sum P_y^Z(n) = f_{AZ}N_0(1-y) \tag{10}$$

So, the oscillator strength of each observed vibrational mode in the ternary AY_yZ_{1-y} generated by the A-Y or A-Z dipoles in the T_n tetrahedron is proportional to the probability of finding the Y (Eqn. 4) or the Z (Eqn. 5) anion belonging to the T_n tetrahedron in the lattice. It means, that the first step in the interpretation of these lines in AY-like and AZ-like sub-bands should be the calculation of the probabilities (4) and (5). The relations between these probabilities corresponding to the relations of oscillator strengths of respective modes will allow us to find, to which tetrahedron T_n belongs each observed mode.

The second important consequence of the VB model in the case of random distribution, is the statement, that the oscillator strength sum for each dipole pair should be proportional to the composition - content of the component AY or AZ (equations (9) and (10)). These equations can serve as verification of the random distribution of atoms in the solid solution lattice.

3.2 Identification of the observed lines The results of the calculations of probabilities $P_y^P(n)$ and $P_y^{As}(n)$ for $GaAs_yP_{1-y}$ ternary solid solutions are presented in Table 3. It is clearly seen from Table 3, that for composition y = 0.01, the maximum value of $P_y^{As}(n)$ is the probability

of finding an atom of As in the tetrahedron T_1 e.g $P_y^{As}(1)$, while other probabilities of $P_y^{As}(n)$ e.g $P_y^{As}(2)$, $P_y^{As}(3)$ and $P_y^{As}(4)$ have negligible values. Indeed, at this composition there is not sufficient material to build tetrehedra with two atoms of As. Moreover, there are not enough As atoms to create tetrahedra with three and four atoms of this element. Conversely, for composition y = 0.94 there is sufficient material to build all kinds of tetrahedra, the maximum value of probability is $P_y^{As}(4)$ while $P_y^{As}(3)$ is considerably smaller, because this tetrahedron needs one atom of phosphorus, however, the lattice contains only 6% of GaP. The $P_y^{As}(2)$ and $P_y^{As}(1)$ probabilities are even smaller, because in these tetrahedra, there must be two and three atoms of P, respectively. In the case of y = 0.15 the maximum value has the $P_y^{As}(1)$ probability too, but the $P_y^{As}(2)$ has a comparable value and the $P_y^{As}(3)$ is not very small. For the composition y = 0.44, the $P_y^{As}(2)$ is the largest among all probabilities $P_y^{As}(n)$, while the others have smaller, but comparable values with $P_y^{As}(2)$. In the case of y = 0.72, the $P_y^{As}(3)$ is the maximum, while others have comparable values too. So, when the composition increases from 0.01 to 0.94, the values of, $P_y^{As}(n)$ reflecting the distribution of the As atoms on the tetrahedra in the GaAsP alloy lattice, are characterized by the shift of the $P_y^{As}(n)$ maximum from T_1 (y = 0.01; 0.15) to T_2 (y = 0.44), to T_3 for y = 0.72, and T_4 for y = 0.94. This shift of the $P_y^{As}(n)$ maximum corresponds to the maxima of the GaAs-like subbands in the $\mathrm{Im}\epsilon(\omega, y)$ curves. It is seen from Figures 2 and 3 (as well as in Table 2), that the maximum amplitude has a line at 270.5 cm^{-1} for y = 0.94 and the other lines observed at 263.5 cm^{-1}, 250 cm^{-1} and 239.5 cm^{-1} have progressively smaller amplitudes. Therefore, the interpretation of these lines is obvious: a mode with a maximum oscillator strength at 270.5 cm^{-1} is generated by Ga-As dipoles in the T_4 tetrahedra (according to the maximal value of the $P_y^{As}(4)$ among the $P_y^{As}(n)$ magnitudes), while the others three are generated at 263.5 cm^{-1}, 250 cm^{-1} and 239.5 cm^{-1} in the T_3, T_2 and T_1 ones, respectively. Similarly, in the case of y = 0.72: the mode with maximum amplitude at 273.3 cm^{-1} is generated by Ga-As dipoles in the T_4 cell, while others are generated at 268 cm^{-1}, 258 cm^{-1} and 248 cm^{-1} by the same dipoles in the T_3, T_2 and T_1 ones, respectively. Therefore, for GaAs-like modes the following sequence is fulfilled: ${}^{GaAs}\omega_4 > {}^{GaAs}\omega_3 > {}^{GaAs}\omega_2 > {}^{GaAs}\omega_1$ in agreement with the work of VB (Ref. [1] Fig. 7).

For y = 0.44 the mode with the maximum amplitude is observed at 272.6 cm^{-1} in the second place in the GaAs-like subband and corresponds to the ${}^{GaAs}\omega_3$. According to the maximal value of probability $P_y^{As}(2)$ the mode with maximal oscillator strength should be generated in the T_2 tetrahedron. Moreover, it must be located in the same subband in the third place on the frequency scale, which corresponds to ${}^{GaAs}\omega_2$. It is seen from Table 3 that the probabilities $P_y^{As}(2)$ and $P_y^{As}(3)$ for y=0.44 have values 0.1821 and 0.1431, respectively. Therefore, amplitudes of the corresponding modes should be approximately equal. This enables us to interpret the observed modes: the line at 279.5 cm^{-1} is generated in the T_4 cell, the line at 272.6 cm^{-1} is generated in the T_3 and the third and fourth lines are observed at 266.4 cm^{-1} and 255 cm^{-1} - in the T_2 and T_1, respectively. Subsequently, the line with the maximum amplitude at y = 0.15 is observed at 264.1 cm^{-1} and it is generated in the T_1 tetrahedron, while the two others are visible at 272.1 cm^{-1} and at 278.3 cm^{-1} - in T_2 and T_3, respectively. For y = 0.01 only one line is observed at 270 cm^{-1} and thus it must refer to T_1. In Ref. 1 (see Fig. 7 in Ref.1)), the following assumption was introduced, namely: the lines observed with maximal amplitude for all compositions were attributed to the T_4 tetrahedron. The statistical approach leads to a different interpretation of the lines observed on the GaAs-like subband.

The distribution of probabilities $P_y^P(n)$ on the tetrahedra is a mirror image of $P_y^{As}(n)$. For composition y = 0.01 the maximal value of probability is $P_y^P(0)$, $P_y^P(1)$ is considerably smaller, because this tetrahedron needs one atom of arsenic, but the lattice contains only 1% of GaAs. The $P_y^P(2)$ and $P_y^P(3)$ probabilities are smaller, because in these tetrahedra, there must be two and three atoms of As, respectively. In the case of y = 0.15 the maximal value among the $P_y^P(n)$ probabilities has also $P_y^P(0)$, while other probabilities such as $P_y^P(1)$, $P_y^P(2)$ and $P_y^P(3)$ have comparable values with $P_y^P(0)$. At y=0.44 this maximum of $P_y^P(n)$ occurs for the $P_y^P(1)$ probability and at y = 0.72 - for $P_y^P(2)$. In the case of y = 0.94, the $P_y^P(3)$ probability has a maximum value, while other magnitudes $P_y^P(2)$, $P_y^P(1)$ and $P_y^P(0)$ have negligible values. The shift of the $P_y^P(n)$ maximum together with the composition change, corresponds to the maximum positions of the GaP-like subbands for different values of y. For example, for the composition y = 0.01, the maximal amplitude appears for the line at 363 cm^{-1}. Other lines have considerably smaller amplitudes and are observed at the softer side of the subband: 353 cm^{-1}, 345 cm^{-1}, 335 cm^{-1}. So, the line at 363 cm^{-1} must be generated by the Ga-P dipoles in the T_0 tetrahedron, while the other three must be caused by the same ion pair in the T_1, T_2 and T_3 tetrahedra, respectively. Analogically, for y = 0.15: the mode with the maximum oscillator strength at 359.5 cm^{-1} is generated by the Ga-P dipoles in the T_0 tetrahedron, while the other three - at 353.4 cm^{-1}, 345.4 cm^{-1} and 336 cm^{-1}, are created by the same dipoles in the T_1, T_2 and T_3 cells, respectively. So, the frequency sequence takes place for GaP-like modes: ${}^{GaP}\omega_0 > {}^{GaP}\omega_1 > {}^{GaP}\omega_2 > {}^{GaP}\omega_3$ contrary to VB[1]. It is necessary to assume, that the line observed at 378 cm^{-1} is located out of the frequency region determined for the GaP-like CPMs frequencies, because the line at 359.5 cm^{-1}, with the maximum amplitude, must be attributed to the ${}^{GaP}\omega_0$ - the CPM with the maximum frequency. Consequently, the line at 378 cm^{-1} should be qualified as an Additional Phonon Mode (APM).

When the composition y = 0.44 is reached, the maximum of the GaP-like subband is at 353 cm^{-1} which, seemingly would correspond to the third position in the mode frequency sequence ($^{GaP}\omega_2$). If we assume, that the line at 371.2 cm^{-1} is an APM (as the line at 378 cm^{-1} for y=0.15), then the line at 353 cm^{-1} belonging to the CPMs frequency consequence is in second place and corresponds to the $^{GaP}\omega_1$ mode generated in the T_1 tetrahedron. Thereafter, the line at 362.2 cm^{-1} corresponds to the $^{GaP}\omega_0$ mode generated in the T_0 tetrahedron, while the lines at 346.3 cm^{-1} and 337 cm^{-1} are generated in the T_2 and T_3 tetrahedra, respectively. At y=0.72, the line observed with its maximal amplitude at 351.3 cm^{-1} should be attributed to the $^{GaP}\omega_2$ CPM generated in the T_2 cell, while the other two lines observed at 358 cm^{-1} and 345.6 cm^{-1} can be attributed to the $^{GaP}\omega_1$ and $^{GaP}\omega_3$ modes, respectively. The line at 362.3 cm^{-1} cannot be interpreted as the $^{GaP}\omega_0$ CPM, because it has a relatively large amplitude, and it is located out of the frequency region of the GaP-like CPMs, e.g. is rather an APM.

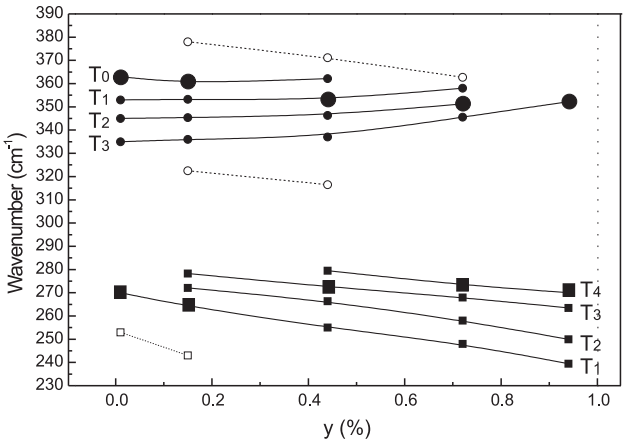

Figure 3 Positions on the frequency scale of the maxima and shoulders observed on Im$\epsilon(\omega, y)$-curves in Fig. 2. Symbols: filled circles - are GaP-like CPMs, filled squares - GaAs-like CPMs, open circles and squares - APMs.

At y = 0.94 only one CPM could be observed, namely $^{GaP}\omega_3$. Therefore the line observed at 352.2 cm^{-1} is interpreted in this way. Hence, the results from the statistical approach, allow us to identify the lines presented in Fig. 3 which is different from the one proposed by VB (Ref. [1], Fig. 7).

3.3 Additional phonon modes The frequency region for CPMs is determined by the maximum value of the CPM frequency (which is the $^{GaP}\omega_0$ for the GaP-like modes and the $^{GaAs}\omega_4$ for the GaAs-like modes) and by the minimum value of the CPMs frequency (which are the $^{GaP}\omega_3$ and the $^{GaAs}\omega_1$ for the GaP-like and GaAs-like modes, respectively). As mentioned above, it is necessary to assume, that the lines at 378 cm^{-1} (y = 0.15), 371.2 cm^{-1} (y = 0.44) are located out of the region determined for the GaP-like CPMs and should be thus attributed to an APM. The same concerns the lines at 322.5 cm^{-1} and 316.5 cm^{-1}. It is possible to assume that the Ga-P dipole oscillations are responsible for these lines.

The APM frequency behavior, which changes with the composition, is different compared to CPMs, as follows from Fig. 3, where the positions of these lines are marked by empty circles and squares. A similar situation takes place in the MCT solid solutions with the lines at 100 - 115 cm^{-1}[18]. This strongly suggests, that the sources of these modes are the Ga-P dipoles in the tetrahedra with the P atom shifted away from the stable position. This is similar to the Hg atoms in the $Hg_{1-x}Cd_xTe$ lattice, where the X-ray diffraction data confirm the hypothesis, that in the MCT lattice there are two energetic minima (model of the two wells potential) for the mercury atoms: the first is stable and deeper and the second is meta-stable and more shallow. The latter one, is characterized by a longer bond with an anion, which automatically means a smaller frequency of oscillations[23]. This could explain the sources of the APM generated by the Ga-P dipole with frequencies smaller than those of the Ga-P CPMs, e.g. the APMs at about 320 cm^{-1}, as well as the weak APMs observed at 240 - 255 cm^{-1} as Ga-As dipole oscillations in the deformed tetrahedra. These APMs do not distort the general picture of the GaAsP phonon spectra.

A different situation occurs in the case of the APMs at 378 cm^{-1} (y = 0.15) and 371.2 cm^{-1} (y = 0.44) with comparably large oscillator strengths. Including these two APMs, as generated by the Ga-P dipoles, in the oscillator strengths sum (see Fig.4 open circles) disturbs the proportionality of the latter one in the GaP content. We should thus assume, that these lines are generated by different sources. The frequency values of these APMs are located in the gap between TO and LO GaP-like phonons. These could be the surface GaP-like phonons or other modes[41].

3.4 Sum of the Oscillator Strengths An important characteristic of the applied approach to the VB model is the sum of the oscillator strengths for each dipole pair. According to Eqn. (9) the sum $\sum S_y^{GaAs}(n) = f^{GaAs}y$, e.g. is proportional to the composition y (GaAs-content), and according to Eqn. (10) the sum $\sum S_y^{GaP}(n) = f^{GaP}(1-y)$, e.g. is proportional to the GaP-content. Therefore, these dependencies can be considered as a verification of the model in the case of the random distribution of atoms. In Table 2, the calculated values of these sums are presented for different compositions (different values of y) and are plotted in Fig. 4 as filled circles for the $\sum S_y^{GaP}(n)$ with additional modes observed for GaP-like sub-band below 330 cm^{-1} (contribution of these APMs into the sum of the oscillator strengths is insignificant), as well as for GaAs-like subband as filled squares (including APMs below 260 cm^{-1} for y= 0.01 and 0.15). It is seen, that in this approach the sum of oscillator strengths $\sum S_y^{GaAs}(n)$ is proportional to the GaAs content in the GaAsP alloy within the limits

of measurement uncertainty. Also the $\sum S_y^{GaP}(n)$ sum is proportional to the GaP content.

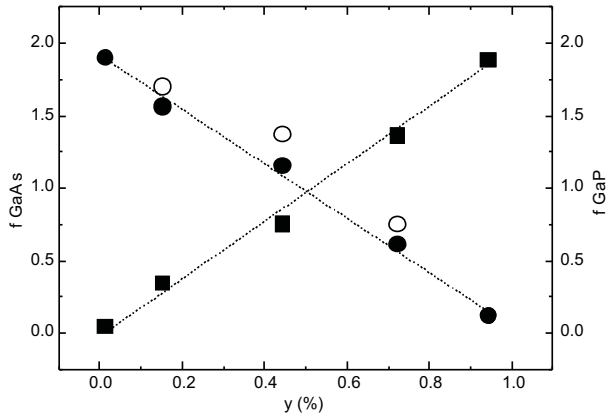

Figure 4 The oscillator strengths sums as functions of composition for the GaAsP solid solutions: filled circles - without APMs higher than 360 cm^{-1}, open circles with APMs.

Deviations from proportionality occur, if the oscillator strengths of the APMs observed at 378 cm^{-1} (y = 0.15) and 371 cm^{-1} (y = 0.44) are included (open circles in Fig. 4) in the oscillator strength sum. So, it is possible to exclude the high frequency APMs as non-related, e.g. not belonging to the family of the GaP-like and GaAs-like TO-modes of the GaAsP alloys.

4 Conclusion The reinterpretation of the GaAsP reflection spectra measured by VB[1] presented in this paper, is based on the model proposed by the authors in Ref 1. This model of five basic structural cells (tetrahedra) was completed by a statistical approach, which enabled us to derive quantitative relations for oscillator strengths of separate lines. The version of the random distribution of atoms in the alloy lattice of the VB model is derived and the rule of the oscillator strengths sum proportionality to the content of the components for each dipole pair is developed as the criterion of random distribution of atoms in the lattice. At the same time, the Additional Phonon Modes (APMs) outside the region of the canonical phonon modes are found in the experimental spectra obtained by VB[1]. These APMs can be divided into two types : i) the same modes as the CPMs, but generated in the deformed tetrahedra, and ii) completely different ones, not belonging to the family of the GaAs-like and GaP-like TO-modes of the $GaAs_yP_{1-y}$ ternary solid solutions. The contribution of the first type of APMs in the sum of the oscillator strengths does not disturb the proportionality of the component content. Including the second type of APMs in this sum, causes a deviation from the proportionality law. So, the latter ones are non-related modes, for example surface modes or other types. Consequently, after a correct identification of the observed lines, it was found that the hypothesis introduced by VB as "clusterisation", caused by an excess of the T_0 and

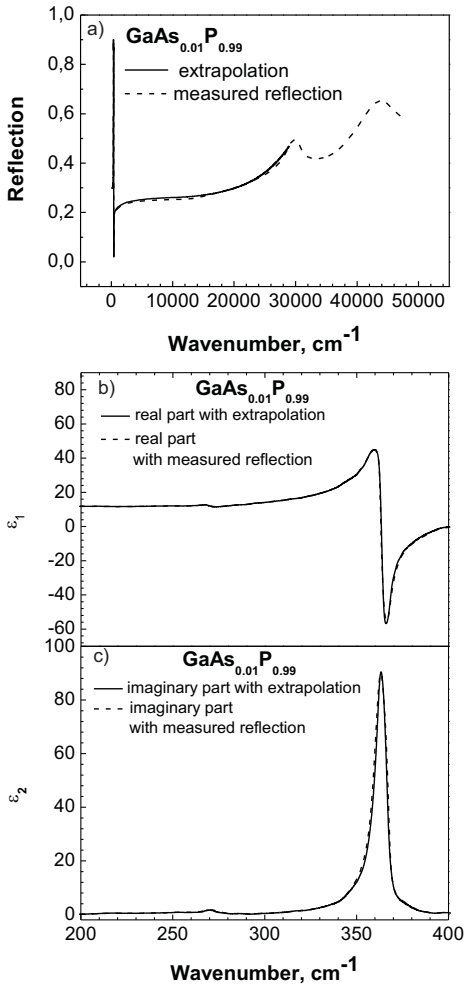

Figure 5 (a) Reflectance case R(ω) for y=0.01: i) the function f(ω)= A(∞)+B(∞) exp($\xi(\infty)\omega$) is used to coalesce two curves - measured in the far infrared region and low-frequency wing in the high-frequency region (solid curve, the part of reflectance measured by VB[1] in the far-infrared region 200 - 400 cm^{-1} appears as a vertical line in the used scale of frequency) and ii) measured reflectance[42] in the region 5 000 - 50 000 cm^{-1} is added (dotted curve); (b) two curves of Re$\epsilon(\omega)$ calculated by K-K transformation for the composition y = 0.01, using the two reflectance curves, as shown in Fig. 7 (a) (c) two curves of Im$\epsilon(\omega)$ calculated by the same way.

T_4 tetrahedra in the lattice (in comparison of the random distribution) is not necessary.

Appendix A Fig. 5 a,b and c presents two reflectance curves R(ω) (a), together with two curves of the real part of the dielectric function Re$\epsilon(\omega)$ (b) and the imaginary part of the dielectric function Im$\epsilon(\omega)$ (c) calculated for the composition of $GaAs_yP_{1-y}$ corresponding to y = 0.01. The solid curve of the Im$\epsilon(\omega)$ in Fig. 5c is shown for the case, when

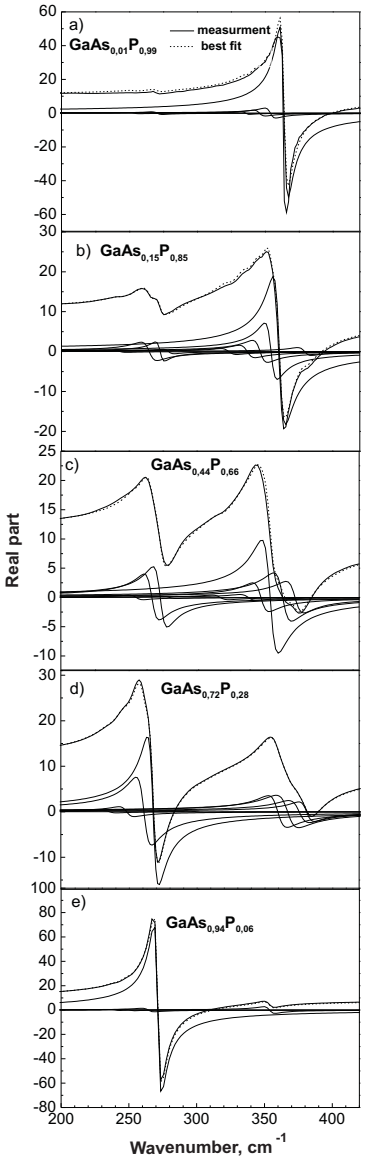

Figure 6 Real parts of the dielectric function Re$\epsilon(\omega, y)$ (solid bold curves) a) y=0.01; b) y=0.15; c) y=0.44; d) y=0.72; f) y=0.94. Thin solid curves are Lorentzians applied for the approximation of the Re$\epsilon(\omega, y)$ curves, bold dotted curves - sum of Lorentzians calculated according to Eqn. (B1). The parameters of Lorentzians are the same as for Im$\epsilon(\omega, y)$ in Fig. 2 and are presented in Table 2. The mean square deviations at approximation was for each curve: (a) $\sigma = 4.18$, (b) $\sigma = 0.49$, (c) $\sigma = 0.21$, (d) $\sigma = 0.14$, (e) $\sigma = 0.75$.

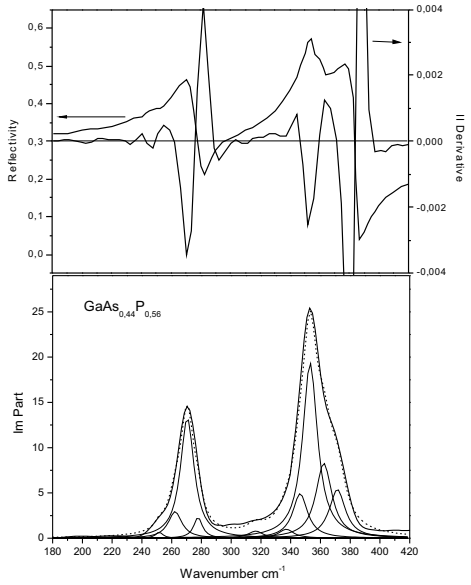

Figure 7 Second derivative $d^2R(\omega)/d\omega^2$ for the y = 0.44 in comparison with the Im$\epsilon(\omega)$ obtained by K-K for the reflectance curve R(ω, 0.44).

the function f$(\omega) = A(\infty) + B(\infty)exp(\xi(\infty)\omega)$ is used to coalesce two curves - the one measured in the far infrared region. The low-frequency wing in the high-frequency region (see reflectance curves in Fig. 5a) is applied to the reflectance R(ω) up to 30000 cm^{-1}. The dotted curve corresponds to the case, when the reflectance curve measured for GaP[42] in the region 30 000 -55 000 cm^{-1} is also included. It is clearly seen, that only slight changes are caused by this inclusion in the phonon frequency region 30 - 400 cm^{-1} while, no differences are observed in the positions and amplitudes of lines.

Analogically, Fig. 5b presents two curves for Re$\epsilon(\omega)$ calculated in these two ways: including and not including the reflectance curve above 30 000 cm^{-1}. No essential changes are observed on the Re$\epsilon(\omega)$ -curve, too.

Appendix B The Re$\epsilon(\omega)$ curves are presented in Fig. 6 (a),(b), (c), (d), and (e) for five compositions of $GaAs_{1-y}P_y$ solid solutions similarly to Fig. 2 which shows the Im$\epsilon(\omega)$ curves. Thin solid curves shown in Fig. 6 (a),(b), (c), (d), and (e) are Lorentzians approximating separate lines of the Re$\epsilon(\omega, y)$ curves according the formula:

$$Re\epsilon(\omega) = \epsilon_\infty + \sum_{i=1}^{k} \frac{S_i \gamma_i (\omega - \omega_{TOi})}{(\omega_{TOi}^2 - \omega^2)^2 + \omega^2 \gamma_i^2} \qquad (11)$$

The theoretical curves calculated by Eqn. (11) are shown for each composition as bold dotted curves. These calculations use the same parameters of oscillators S_i, ω_{TOi} and γ_i as those used for calculations of the Im$\epsilon(\omega)$

curves (see Fig. 2) and are presented in Table 2. It is possible to see, that the theoretical curves of the imaginary part of dielectric function approximate very well the experimental ones obtained by K-K transformation of the reflectance curves measured in Ref.1. Therefore, only the one set of oscillator parameters enables us to approximate the Re$\epsilon(\omega)$ and Im$\epsilon(\omega)$ curves simultaneously.

Fig. 7 presents the result of numerical differentiating of the R(ω)-curve for y=0.44 - $d^2R(\omega)/d\omega^2$. A comparison with Im$\epsilon(\omega)$ curves shows that the weak peculiarities on the reflectance curve are emphasized simultaneously by differentiating as well as by K-K transformation. It is seen, that practically to each zero-point on the $d^2R(\omega)/d\omega^2$-curve is corresponding to a Lorentzian approximating the Im$\epsilon(\omega)$ -curve.

References

[1] H.W.Verleur and A.S.Barker, Phys.Rev., **149**, 715 (1966).
[2] H.W.Verleur and A.S.Barker, Phys. Rev., **155**, 750 (1967).
[3] M. Ilegems and G. L. Pearson, Phys. Rev. B **1**, 1576 (1970).
[4] O.K. Kim and W.G. Spitzer, J. Appl. Phys. **50**, 4362 (1979).
[5] H. Ono and T.Baba, Phys. Rev. B **42**, 11423 (1990).
[6] S.P. Kozyrev, L.K. Vodopyanov, R. Triboulet, Solid State Commun. **45**, 383 (1983).
[7] S.P. Kozyrev, L.K. Vodopyanov, R. Triboulet, Phys. Rev. B **58**, 24, 1374 (1998).
[8] J. M. Wrobel, B. P. Clayman, P. Becla, R. Sudharsanan, and S. Perkowitz J. Appl. Phys., **64**, 310 (1988).
[9] S. Perkowitz, L. S. Kim, Z. C. Feng, and P. Becla Phys. Rev. B **42** 1455, (1990).
[10] S. Perkowitz, L. S. Kim, and P. Becla, Phys.Rev. B **43**, 6598 (1991).
[11] P. N. Sen, G. Lucovsky, Phys. Rev. B **12**, 2998, (1975).
[12] E. M. Sheregii, J. Polit, J. Cebulski, A. Kisiel, B. V. Robouch, A. Marchelli, M. Cestelli Guidi, M. Piccinini, Infrared Physics, **49**, 13 (2006).
[13] J. Polit , E. M. Sheregii, J. Cebulski, B. V. Robouch, A. Marchelli, M. Cestelli Guidi, M. Piccinini, A. Kisiel, P. Zajdel, E. Burattini, A. Mycielski, J. Appl. Phys. **100**, 013521-1-10 (2006).
[14] J. Polit , E. M. Sheregii, J. Cebulski, B. V. Robouch, A. Marchelli, M. Cestelli Guidi, M. Piccinini, A.Kisiel, Infrared Physics, **49**, 23 (2006).
[15] J. Cebulski, E. M. Sheregii, J. Polit, A. Kisiel, B. V. Robouch, A. Marchelli, M. Cestelli Guidi, M. Piccinini, Infrared Physics, **49**, 19 (2006).
[16] J. Cebulski, E. M. Sheregii, J. Polit, A. Marcelli, M. Piccinini, A. Kisiel, I. Kucherenko, R. Triboulet, Appl. Phys. Lett. **92**, 121904 (2008).
[17] E. M. Sheregii, J. Cebulski, A. Marcelli and M. Piccinini, Phys. Rev. Lett. **102**, 045504 (2009).
[18] J. Polit, E. M. Sheregii, J. Cebulski, A. Kisiel, A. Marcelli, B. Robouch, A. Micielski, Phys. Rev. B **82**, 014306-1-12 (2010).
[19] B.V.Robouch, A.Kisiel, J.Konior, J. Alloys Compounds, **339**, 1 (2002).
[20] B.V.Robouch, A.Kisiel, E.M.Sheregii, Phys. Rev. B **64**, 73204 (2001).
[21] B.V.Robouch, A.Kisiel, J.Konior, J. Alloys Compounds **340**, 13 (2002).
[22] Zhonghua Wu, Kunquan Lu, Yuren Wang, Jun Dong, Hefeng Li, Chenxi Li and Zhengzhi Fang, Phys. Rev. B **48**, 8694 (1993).
[23] O. Pages, J. Souhabi, A. V. Postnikov, and A. Chafi, Phys. Rev. B **80**, 035204 (2009).
[24] M. Cardona, Modulation Spectroscopy, Academic Press, New York, 1969.
[25] S. Adachi, Optical Properties of Crystalline and Amorphous Semiconductors. Materials and Fundamental Principles, Kluver Academic Publishers, Boston, 1999.
[26] K.G. Hambleton, C Hilsum and B.R. Holeman, Proc. Phys. Soc., **77**, 1147 (1961).
[27] C.J. Johnson, G.H. Sherman and R.Weil, Appl. Opt., **8**, 1667 (1969).
[28] A.H. Kachare, W.G. Spitzer, F.K. Euler, and A. Kahan, J. Appl. Phys., **45**, 2938 (1974).
[29] R.T. Holm, J.W. Gibson and E.D. Palik, J. Appl. Phys. **48**, 212 (1977).
[30] J.S. Blakemore, J. Appl. Phys., **53**, R123 (1982).
[31] G.A. Samara, Phys. Rev. B **27**, 3494 (1983).
[32] W.J. Moore and R.T. Holm, J. Appl. Phys., **80**, 6939 (1996).
[33] D.A. Kleinman, and W.G. Spitzer, Phys. Rev., **118**, 110 (1960).
[34] M. Haas, B.W. Henvis, J. Phys. Chem. Sol.,**23**, 1099 (1962).
[35] M. Hass, Semiconductors and Semimetals, ed. by R.K. Willardson and A. Beer; vol. 3, Optical properties of III-V oleman, Appl. Opt. 10, 1683, (1971).
[36] D.F. Parson and P.D. Coleman, Appl. Opt. **10**, 1683, (1971).
[37] Bruker Analytische, Messtachnik, GmbH. OPUS/IR Reference Manual, Version 2.0; Bruker Analytische Messtechnik, GmbH: Karlsruhe, Germany, 1995.
[38] The same procedure of K-K transformation was applied to R(ω)-curves in our published works Refs.12-17.
[39] J.M. Ziman, Models of disorder, Cambridge University Press, Cambridge, England, 1979.
[40] B.I. Lundqvist, Physik der Kondensierten Materie **6**, 193 (1967); **6** 206 (1967); **7** 117 (1968); **9** 236 (1969).
[41] The modes at 371-378 cm^{-1} were observed by other authors who investigated the GaAsP alloys phonon spectra: see I.F. Chang and S.S. Mitra, Phys. Rev. **172**, 924 (1968) where the reflection spectra are published, and the Kramers-Kronig transformation show the same lines at 371-378 cm^{-1} or the results on Raman scattering obtained for two-dimensional structures with GaAsP (see M. I. Alonso, P. Castrillo, G. Armelles, A. Ruiz, M. Recio, and F. Briones, Phys. Rev. B **45**, 9054 (1992).
[42] D. E. Aspnes and A. A. Studna, Phys. Rev. B **27**, 985 (1983) it is justified to assume, that resonances caused by the electron structure in the high frequency region (correspondingly a reflectance curve in this region also) are practically the same for GaP and $GaP_{1-y}As_y$ if y=0.01.

Table 2 Parameters of Lorentzian's oscillators used for fitting the Im$\epsilon(\omega, y)$ curves.

y	Number of Line	S_i,cm^{-2}	ω_{Toi}, cm^{-1}	γ_i, cm^{-1}	$\sum_i \frac{S_i^{GaAs}}{(\omega_i^{GaAs})^2}$	$\sum_i \frac{S_i^{GaP}}{(\omega_i^{GaP})^2}$
	1	1500 ±100	253 ±0.5	9.0 ±0.5	0.07	
	2	3500 ±200	270 ±0.5	8.0 ±0.3	0.07	
	3	3000 ±200	335 ±0.5	6.0 ±0.3		1.91
0.01	4	9700 ±500	345 ±0.5	8.2 ±0.4		
	5	16800 ±900	353	8		1.91 ±0.5
	6	220000 ±2000	363 ±0.5	7.0 ±0.1		
	1	1000 ±100	243 ±0.5	10.0 ±0.8		
	2	14000 ±500	264.1 ±0.5	11.5 ±0.3	0.36	
	3	8500 ±300	272.1 ±0.5	10.5 ±0.3		
	4	2500 ±200	278.3 ±0.5	8.0 ±0.5		
0.15	5	5500 ±300	322.5 ±0.5	11.5 ±0.5		
	6	12000 ±400	336 ±0.5	11.5 ±0.3		
	7	21000 ±800	345.4 ±0.5	11.0 ±0.6		
	8	45000 ±1000	353.4 ±0.5	9.0 ±0.4		1.68
	9	120000 ±1300	359.5 ±0.5	9.0 ±0.2		
	10	7500 ±500	378±0.5	10.0 ±0.6		
	1	2000 ±200	255 ±0.5	10.0 ±0.5		
	2	23000 ±800	266.4 ±0.5	11.0 ±0.3		
	3	29000 ±500	272.6 ±0.5	10.3 ±0.2	0.76	
	4	1000 ±100	279.5 ±0.5	10.0 ±0.7		
0.44	5	3000 ±100	316.5 ±0.5	12.0 ±0.5		
	6	4000 ±400	337 ±0.5	12.0 ±0.9		
	7	20500 ±1000	346.3 ±0.5	12.0 ±0.4		1.38
	8	82000 ±500	353 ±0.5	12.0 ±0.2		
	9	39000 ±800	362.2 ±0.5	13.0 ±0.3		
	10	26000 ±500	371.2 ±0.5	13.0 ±0.3		
	1	1000 ±100	248 ±0.5	8.0 ±0.5		
	2	5000 ±300	258 ±0.5	8.9 ±0.6	1.37	
	3	36000 ±1000	268 ±0.5	9.0 ±0.4		
0.72	4	58000 ±1500	273.3 ±0.5	6.5 ±0.2		
	5	26500 ±800	345.6 ±0.5	11.0 ±0.5		
	6	32500 ±600	351.3 ±0.5	13.0 ±0.2		0.75
	7	21000 ±500	358 ±0.5	12.1 ±0.3		
	8	14000 ±600	362.3 ±0.5	9.0 ±0.5		
	1	1000 ±100	239.5 ±0.5	6.0 ±0.9		
	2	2000 ±200	250 ±0.5	7.0 ±0.9	1.89	
0.94	3	7000 ±600	263.5 ±0.5	9.0 ±0.9		
	4	127000 ±1000	270.5 ±0.5	5.5 ±0.2		
	5	15500 ±1000	352.2 ±0.5	8.0 ±0.5		0.12

Table 3 Probabilities to find the As and P atoms in T_n tetrahedron in the GaAsP alloy lattice.

y	T_0		T_1		T_2		T_3		T_4	
	$P_y^P(0)$	$P_y^{As}(0)$	$P_y^P(1)$	$P_y^{As}(1)$	$P_y^P(2)$	$P_y^{As}(2)$	$P_y^P(3)$	$P_y^{As}(3)$	$P_y^P(4)$	$P_y^{As}(4)$
0.01	0.9606		0.0291	0.0097	0.0003	0.0003	9.9E-7	2.9E-6		1E-8
0.15	0.5220		0.2763	0.0921	0.0488	0.0488	0.0029	0.0086		0.0005
0.44	0.0983		0.2318	0.0773	0.1821	0.1821	0.0478	0.1431		0.0375
0.72	0.0061		0.0474	0.0158	0.1219	0.1219	0.1045	0.3135		0.2687
0.94	1.3E-5		0.0006	0.0002	0.0095	0.0095	0.0498	0.1495		0.7807